Broadband Zero-Bias RF Field-Effect Rectifiers Based on AlGaN/GaN Nanowires

Giovanni Santoruvo, Mohammad Samizadeh Nikoo, and Elison Matioli, *Member, IEEE*

Abstract—**Microwave zero-bias rectifiers are fast devices capable of rectifying RF signals without applied bias, which have applications ranging from RF power detection to THz imaging systems. Here we present gated nanowire field-effect rectifiers (NW-FERs) fabricated with a process compatible with other RF devices on a standard AlGaN-GaN High Electron Mobility Transistor (HEMT) platform as a new potential RF zero-bias diode. Signal rectification relies on the electrostatic modulation of the gated-NW carrier concentration, which is optimized by a judicious NW width design. NW-FERs presented a large curvature (30.1 V^{-1}), close to the theoretical limit (38.7 V^{-1}) for ideal Schottky diodes, and an excellent trade-off between a flat frequency response, up to a few tens of GHz, and a large responsivity (3000 V/W). The compatible fabrication process and the very good results provide a promising high-performance zero-bias diode architecture that could be integrated on AlGaN/GaN microwave monolithic integrated circuits (MMICs).**

Index Terms—**Nanowire, RF zero-bias diode, THz imaging, RF power detection.**

I. INTRODUCTION

GAN-based high electron mobility transistors (HEMTs) are one of the most promising platforms for the development of MMICs, for which the integration of microwave power detectors could enable both an improved performance as well as new applications. Microwave power detectors are devices generating a DC voltage proportional to the RF signal power at their input. Applications include incoherent demodulation by envelope detection, demodulation based on six-port receivers [1]–[3], terahertz imaging [4]–[6] and power monitoring to improve the efficiency of power amplifiers[7]–[9].

Detectors operating without the need for DC bias, called zero-bias detectors, are very favorable for these applications since they ensure a sharp reduction of the shot and flicker (1/f) noise, and do not require energy nor DC biasing networks to operate [10].

Excellent RF detection performances have been reached with optimized Schottky contacts on heavily engineered epitaxial structures based on n/n$^+$-GaAs [11], [12], as well as in Sb-based tunnel junctions [13]–[18], however they are not compatible with current MMIC epitaxial structures.

Zero-bias detectors based on AlGaN/GaN HEMTs have been demonstrated using nanoscale devices, such as self-switching diodes (SSDs) presenting very high-frequency operation (up to hundreds of GHz) [19]–[21], as well as in lateral

field-effect diodes (L-FEDs) showing excellent detection capabilities (responsivity in the order of thousands of V^{-1}) [10], [22]–[24]. Devices based on GaN HEMT structures presenting concurrently good detection and frequency capabilities would expand the portfolio of RF devices for GaN MMICs. In this letter, we demonstrate zero-bias NW-FERs, based on an array of tri-gated nanowire HEMTs (Fig. 1a-d), presenting excellent zero-bias rectification performance. Zero-bias field-effect rectifiers (Fig. 1b) require the channel threshold voltage (V_{th}) to be positive and close to 0 V [22], [25]. By using NWs as channel (Fig. 1c), V_{th} could be finely tuned with high precision and reproducibility to obtain a V_{on} close to 0 V. The tri-gates resulted in a steep sub-threshold slope, which was exploited to enhance the rectification capabilities of the devices [26], obtaining detection performance approaching the behavior of ideal field effect rectifiers and Schottky diodes used as RF detectors [27].

NW-FERs are first analyzed in DC, highlighting the influence of V_{TH} on DC figures of merit. Then, responsivity measurements, both versus input power (P_{in}) and frequency (f), are shown and discussed. Finally, S-parameters are reported together with the equivalent circuit model.
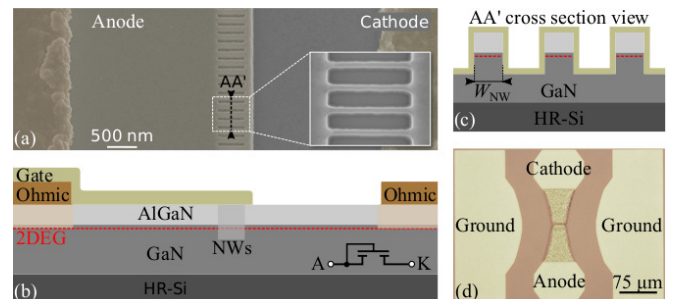

Fig. 1. (a) SEM image of a 30 nm-wide NW-FER. The inset shows the NW array before gate metal deposition. (b) Lateral and (c) cross-section (along AA') schematics of the device. (d) Optical image of a NW-FER showing the ground-signal-ground (GSG) pads for RF measurements.

II. RESULTS AND DISCUSSION

NW-FERs were fabricated on GaN (2.7 nm)/ AlGaN (25 nm)/GaN (500 nm) followed by a 1.7 μm-thick buffer on high-resistive silicon substrate. The electron mobility (μ_e), carrier concentration (n_s) and sheet resistance (R_{sh}) of the epitaxial structure measured at 300 K were 1917 cm^2/Vs, 1.06×10^{13}cm^{-2} and 300 $\Omega/\square$, respectively. NW-FERs were fabricated by electron-beam lithography using hydrogen silsesquioxane 2% (HSQ), followed by Cl$_2$-based dry-etching
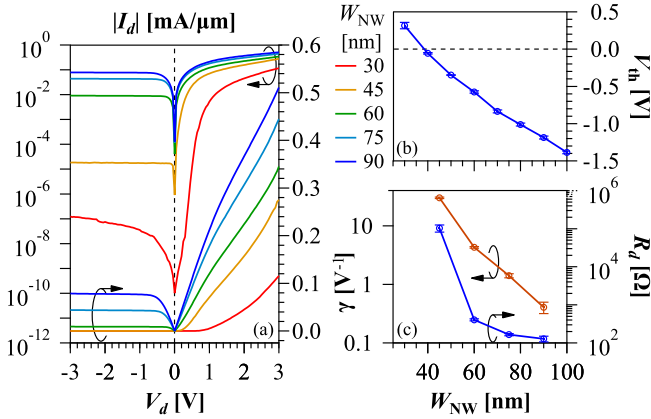
Fig. 2. (a) Diode current $|I_d|$ versus voltage V_d in logarithmic (left axis) and linear (right axis) scales for NW-FERs with NW widths of 30 nm, 45 nm, 60 nm, 75 nm and 90 nm. (b)V_{th} (defined at 1 μA/mm) for Schottky tri-gate HEMTs versus NW width. (c) γ and R_d at $V_d = 0$ V for NW-FER with NW width from 45 nm to 90 nm (devices with 30 nm wide NWs are not shown since they cannot work as zero bias diode due to the large V_{on}).

of the nanowires and mesa isolation. Ohmic contacts were formed by Ti (200 Å)/Al (1200 Å)/Ti (400 Å)Ni (600 Å)/Au (500 Å) annealed at 780 °C, resulting in a contact resistance of 0.81 Ωmm, and Ni (300 Å)/ Au (1300 Å) was used as gate for NW arrays.

Fig. 2a shows the DC performance of NW-FERs, composed of 240 NWs with a length of 500 nm, widths (W_{NW}) varying from 30 nm to 90 nm and a constant NW spacing of 100 nm, which corresponds to a variation of the NW filling factor from 23% to 47%. The device current was normalized by the width of the entire device footprint (not by the NW width).

The NW width plays a key role in defining both the V_{on} and the reverse leakage current (I_r). Narrow NWs (30 nm-wide) presented a much reduced I_r, down to 100 nA/mm, but with large V_{on} of around 0.4±0.05 V (at 1 mA/mm), while wider nanowires (90 nm-wide) presented V_{on} close to 0 V but with much larger leakage current, on the order of the forward current, which significantly degraded the device rectification capability. A good compromise was achieved for devices with 45 nm-wide NWs, with V_{on} of $\sim$0 V and a flat I_r of 20 μA/mm.

Both V_{on} and I_r are directly related to the V_{th} of the NWs, which can be easily tuned from -1.2 V to + 0.4 V by varying the NW width from 90 nm to 30 nm (Fig. 2b). Such dependence is produced by the sidewall depletion of carriers [28], strain relaxation of the barrier layer in narrow NWs [29] (which depends also on the NW length [30]) and the enhanced gate control from the tri-gate structures [26].

V_{th} has also a strong impact on the device detection capability, which is characterized by the current curvature $\gamma = d^2 I_d/dV_d^2(dI_d/dV_d)^{-1}$ [16], and by the differential resistance R_d, both at 0 V. For RF power detectors, low values of R_d are desirable for low thermal noise, along with high values of γ for good power detection. Fig. 2c shows the trade-off between γ and R_d, which are both heavily influenced by W_{NW}. While the 45 nm-wide NW-FERs show the largest γ of 30.1±0.9 V^{-1}, their high R_d can be reduced by increasing the number of NWs and by fine tuning W_{NW} using wet etch treatments [31], [32]. For instance, R_d was reduced by a factor

of 5-6x when increasing the number of NWs from 120 to 240 and a few nm of W_{NW}.

For $V_{th} \ll 0$ V values (large W_{NW}), devices work in the triode-region (high conductive region allowing small R_d) where the current can be modeled as $I_d \propto (V_d/2 - V_{th})V_d$, so γ is equal to $-V_{th}^{-1}$, which leads to a maximum γ of a few V^{-1} [33]. When V_{th} approaches 0 V, devices work in the sub-threshold region (low conductive region) and the current can be modeled as $I_d^{\text{sub-th}} \propto \exp\left(-q\frac{V_{th}}{k_bT}\right)\left(\exp\left(\frac{qV_d}{k_bT}\right)-1\right)$, where q is the elementary charge, k_b is the Boltzmann constant and T is the absolute temperature, resulting in a maximum γ of $q/k_bT =$38.7 V^{-1} [33]. This result resembles Schottky diodes ($\gamma = q/nk_bT$ for which n is the ideality factor), so 45 nm-wide NW-FERs have γ close to the theoretical limit, thanks to the strong channel control of the tri-gate, and they behave similarly to Schottky diodes with n= 1.28. Larger values of γ can be achieved by exploiting different physical phenomena than field effect or Schottky barrier rectification, as in tunnel backward diodes [16].

Fig. 3a shows the rectified V_{out} versus P_{in} at 1 GHz for all devices. The 30 nm-wide NW-FERs could not detect signals below -10 dBm due to their large V_{on}, thus they are not considered for further analysis. The measurement setup used for the responsivity measurement is shown in the inset of Fig. 3.a. The reported P_{in} refers to the power set in the vector network analyzer (VNA) after removing the insertion losses (IL) from the input cable ($P_{in} = P_{in}^{\text{VNA}} - IL_{\text{cable}}$). V_{out} has a linear behavior for a large range of P_{in}, in agreement with the "square-law" of diodes ($V_{out} \propto V_{in}^2 \propto P_{in}$) [34]. At larger P_{in} the impedance of diodes starts to depend on P_{in} causing the sub-linear behavior observable in Fig. 3a [34]. The minimum detectable power generating a stable V_{out}, measured using a multimeter (which represents a real application case), was -50 dBm for 45 nm-wide NW-FERs, which was degraded for wider NWs devices. The dynamic range was about 30 dBm (calculated from the 1 dB compression point) independently from the NW widths.

Fig. 3b shows β, defined as V_{out}/P_{in}, for all devices versus P_{in}, revealing a significant increase of up to 2 orders of magnitude for narrow NW-FERs, which is a consequence of the much larger γ (Fig. 2a). The 45 nm-wide NW-FERs presented a maximum β of 3000 V/W, which is very close to the theoretical value of $2Z_s\gamma = 3010$ V/W, defined in the case of complete mismatch between the device impedance ($\sim$ 100 kΩ) and the source impedance Z_s (50 Ω of the VNA port) [33]. At large power, the responsivity approaches the theoretical value of $2\sqrt{2Z_0/P_{in}}$, which considers a capacitive load connected to an ideal diode in off-state ($I_r = 0$ A), for which the entire reflected power causes the doubling of input voltage. Therefore, NW-FERs provide good responsivities, in the same order ($>$ 1000 V/W) of those for state of the art devices [10], [12], [14]–[16], [35], on a platform compatible to RF GaN HEMTs. Such results were achieved without any matching network, allowing a simpler and more compact design as well as broader band operation.

Fig. 4a shows the measured frequency response of β at P_{in} = -20 dBm (square law region for all devices) for a large
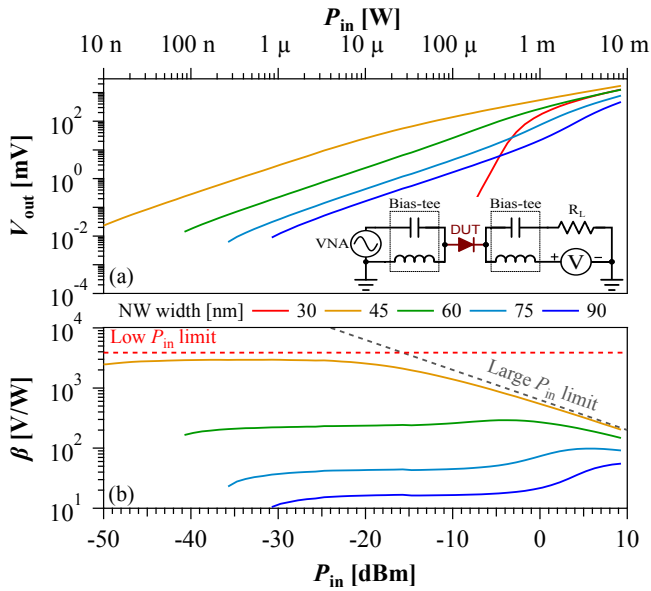
Fig. 3. (a) V_{out} and (b) β versus P_{in} at 1 GHz. Inset: Schematic of the measurement setup for RF detection. Losses in measurement cables have been compensated for a precise determination of β.

Fig. 4. (a) β versus input signal frequency at P_{in} = -15 dBm. (b) Measured (solid blue) and modeled (dashed red) S_{11} and S_{12} of a 45 nm-wide NW-FER. Inset: Equivalent circuit model of the device with values obtained from S-parameter measurement fitting.

frequency range, up to 50 GHz. The 45 nm-wide NW-FERs showed a large and flat β over almost the entire measured range, corresponding to an improved frequency performance compared to other lateral FERs [24] together with a very good responsivity. The oscillations seen in Fig. 4a are due to impedance mismatches between the devices and the VNA.

The S-parameters of 45 nm-wide NW-FERs were measured (Fig. 4b) to extract the equivalent circuit parameters (inset of 4b) defining the impedance matrix shown in Eq. 1:

$$Z_{DUT} = \begin{bmatrix} Z_{FER} & -Z_{FER} \\ -Z_{FER} & Z_{FER} \end{bmatrix}; Z_{FER} = R_s + R_j // (j\omega C_j) \quad (1)$$

The fluctuations observed in S_{21} at low frequency are due to the higher noise in the VNA at low frequency and the very low power transmitted through the device. The equivalent circuit element extraction, after open-short de-embedding, resulted in an R_s of 37.9 ±1.6 Ω, a junction resistance R_j of 101 ±17.5 kΩ (similar to the DC $R_d = R_s + R_j \sim R_j$ since $R_j \gg R_s$) and junction capacitance C_j of 30.6 ±1.7 fF for the 45 nm-wide NW-FERs. S-parameter simulations performed using these parameters show a very good match with the measured ones (Fig. 4.b). In addition, we use these circuit parameters to determine the cut-off frequency, defined as $f_c = 1/(2\pi C_j R_s)$ [16], obtaining a value of 140 GHz. The cut-off frequency can be significantly improved by reducing R_s and C_j with an optimized geometry, smaller anode and cathode access regions and reduced contact resistances.

The characterization of zero-bias rectifiers also required considerations about the thermal noise generated and rectified by the device itself. This is described by the noise-equivalent power (NEP), which considers the amount of self-generated rectified thermal noise per unit of frequency that produces a DC value at the output. NEP is equal to $\sqrt{4k_B T R_0}/\beta$, where R_0 is the DC resistance of the device at zero bias. Differently from other reports [20], [36], we believe that the correct value for R_0 should be $R_s + R_j$ obtained from the S-
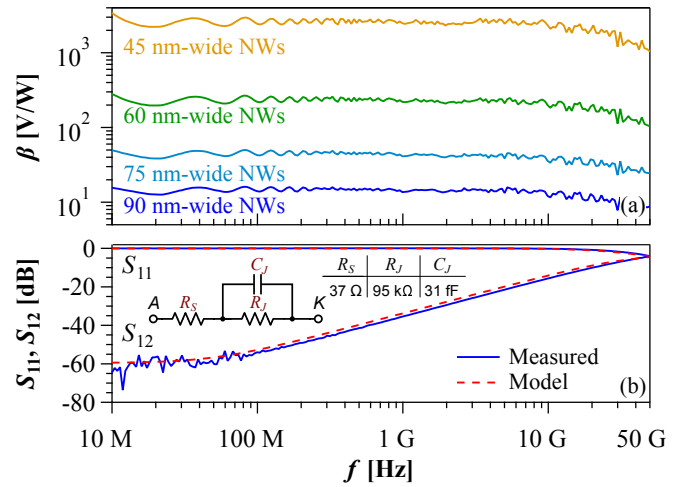
parameters, since it represents the real resistance that generates thermal noise when the device is working at a certain power and frequency. With this definition, a NEP of 18.7 ± 2.3 pW/$\sqrt{Hz}$ was obtained at 1 GHz for P_{in} = -20 dBm, which is more than 30 % smaller than that for devices with 120 NWs ($\sim$27 pW/$\sqrt{Hz}$), showing that increasing the number of parallel NWs, thus reducing the device resistance, can effectively reduce the effect of thermal noise.

CONCLUSIONS

In conclusion, we demonstrated high-performance zero-bias RF rectifiers based on NW-FERs fabricated on a commercial AlGaN/GaN HEMT. The use of NWs offered a flexible design tool and much-improved rectification capabilities. By adjusting the width of NWs, V_{th} could be properly designed, with very high reproducibility, which resulted in a normally-off channel with low V_{on} (required for zero-bias operation in FERs). The tri-gate structure wrapping the NWs yielded a much better channel control than in planar FERs, resulting in a curvature coefficient of 30.1 V^{-1}, which is close to the theoretical limit of 38.7 V^{-1}. NW-FERs showed a large responsivity of 3000 V/W, as predicted by the used model, with a flat frequency response, and a high f_c of 140 GHz. Such value can be significantly improved by reducing R_s and C_j with an optimized geometry and which opens opportunities for high-frequency detectors. The large responsivity reported together with the good frequency response shows that NW-FERs are an excellent alternative to GaN-HEMT-based SSDs and lateral FERs, thus further expanding the device portfolio compatible with GaN MMICs.

REFERENCES

[1] A. Kolpin, S. Winter, R. Weigel, and T. Eireiner, "A sixport receiver's analog front-end for the K-band based on a rapid-prototyped PCB," in *MELECON 2006 - 2006 IEEE Mediterranean Electrotechnical Conference*, May 2006, pp. 360–362.

[2] J.-R. Yang and S. Hong, "A 24-GHz radar sensor with a six-port network for short-range detection," *Microwave and Optical Technology Letters*, vol. 56, no. 11, pp. 2634–2637, 2014. [Online]. Available: https://onlinelibrary.wiley.com/doi/abs/10.1002/mop.28665

[3] H. L. Lee, S. Moon, M. Lee, and J. W. Yu, "Six-port QPSK demodulator for optimal K-band multiport amplifier calibration," *Electronics Letters*, vol. 50, no. 8, pp. 617–618, Apr. 2014.

[4] K. Y. Xu, Y. N. Wang, C. J. Zheng, J. W. Xiong, and G. Wang, "Terahertz Performance of a GaN-Based Planar Nanochannel Device," *Journal of Nanomaterials*, vol. 2014, p. e850915, Apr. 2014. [Online]. Available: http://www.hindawi.com/journals/jnm/2014/850915/abs/

[5] S.-P. Han, H. Ko, J.-W. Park, N. Kim, Y.-J. Yoon, J.-H. Shin, D. Y. Kim, D. H. Lee, and K. H. Park, "InGaAs Schottky barrier diode array detector for a real-time compact terahertz line scanner," *Optics Express*, vol. 21, no. 22, p. 25874, Nov. 2013. [Online]. Available: https://www.osapublishing.org/oe/abstract.cfm?uri=oe-21-22-25874

[6] C. Balocco, Y. Pan, S. R. Kasjoo, Y. Alimi, L. Q. Zhang, and A. M. Song, "THz imaging with broadband thermal sources," in *2014 39th International Conference on Infrared, Millimeter, and Terahertz waves (IRMMW-THz)*, Sep. 2014, pp. 1–2.

[7] A. Tessmann, A. Leuther, H. Massler, S. Wagner, F. Thome, M. Schlechtweg, and O. Ambacher, "A millimeter-wave low-noise amplifier MMIC with integrated power detector and gain control functionality," in *2016 IEEE MTT-S International Microwave Symposium (IMS)*, May 2016, pp. 1–3.

[8] B. Sahu and G. Rincon-Mora, "A High-Efficiency Linear RF Power Amplifier With a Power-Tracking Dynamically Adaptive Buck-Boost Supply," *IEEE Transactions on Microwave Theory and Techniques*, vol. 52, no. 1, pp. 112–120, Jan. 2004. [Online]. Available: http://ieeexplore.ieee.org/document/1262682/

[9] K. A. Lee, D. H. Lee, J. Park, H.-m. Yoo, and S.-H. Cheon, "A InGaP / GaAs HBT WLA with Power Detector," 2004.

[10] Q. Zhou, K. Wong, W. Chen, and K. J. Chen, "Wide-Dynamic-Range Zero-Bias Microwave Detector Using AlGaN/GaN Heterojunction Field-Effect Diode," *IEEE Microwave and Wireless Components Letters*, vol. 20, no. 5, pp. 277–279, May 2010.

[11] L. Liu, J. L. Hesler, H. Xu, A. W. Lichtenberger, and R. M. Weikle, "A Broadband Quasi-Optical Terahertz Detector Utilizing a Zero Bias Schottky Diode," *IEEE Microwave and Wireless Components Letters*, vol. 20, no. 9, pp. 504–506, Sep. 2010.

[12] J. L. Hesler and T. W. Crowe, *Responsivity and Noise Measurements of Zero-Bias Schottky Diode Detectors*.

[13] P. Chahal, F. Morris, and G. Frazier, "Zero bias resonant tunnel Schottky contact diode for wide-band direct detection," *IEEE Electron Device Letters*, vol. 26, no. 12, pp. 894–896, Dec. 2005.

[14] N. Su, Z. Zhang, R. Rajavel, P. Deelman, J. N. Schulman, and P. Fay, "Scaling of High-Performance InAs/AlSb/GaSb Heterostructure Detectors for Millimeter-Wave and Submillimeter-Wave Sensing and Imaging," in *2008 Device Research Conference*, Jun. 2008, pp. 123–124.

[15] H. P. Moyer, J. N. Schulman, J. J. Lynch, J. H. Schaffner, M. Sokolich, Y. Royter, R. L. Bowen, C. F. McGuire, M. Hu, and A. Schmitz, "W-Band Sb-Diode Detector MMICs for Passive Millimeter Wave Imaging," *IEEE Microwave and Wireless Components Letters*, vol. 18, no. 10, pp. 686–688, Oct. 2008.

[16] Z. Zhang, R. Rajavel, P. Deelman, and P. Fay, "Sub-Micron Area Heterojunction Backward Diode Millimeter-Wave Detectors With 0.18 pW/Hz^1/2 Noise Equivalent Power," *IEEE Microwave and Wireless Components Letters*, vol. 21, no. 5, pp. 267–269, May 2011.

[17] M. Patrashin, N. Sekine, A. Kasamatsu, I. Watanabe, I. Hosako, T. Takahashi, M. Sato, Y. Nakasha, and N. Hara, "GaAsSb/InAlAs/InGaAs Tunnel Diodes for Millimeter Wave Detection in 220330-GHz Band," *IEEE Transactions on Electron Devices*, vol. 62, no. 3, pp. 1068–1071, Mar. 2015.

[18] S. M. Rahman, Z. Jiang, M. I. B. Shams, P. Fay, and L. Liu, "A G-Band Monolithically Integrated Quasi-Optical Zero-Bias Detector Based on Heterostructure Backward Diodes Using Submicrometer Airbridges," *IEEE Transactions on Microwave Theory and Techniques*, vol. 66, no. 4, pp. 2010–2017, Apr. 2018.

[19] A. M. Song, M. Missous, P. Omling, A. R. Peaker, L. Samuelson, and W. Seifert, "Unidirectional electron flow in a nanometer-scale semiconductor channel: A self-switching device," *Applied Physics Letters*, vol. 83, no. 9, p. 1881, 2003. [Online]. Available: http://scitation.aip.org/content/aip/journal/apl/83/9/10.1063/1.1606881

[20] P. Sangar, G. Ducournau, B. Grimbert, V. Brandli, M. Faucher, C. Gaquire, A. iguez-de-la Torre, I. iguez-de-la Torre, J. F. Millithaler, J. Mateos, and T. Gonzlez, "Experimental demonstration of direct terahertz detection at room-temperature in AlGaN/GaN asymmetric nanochannels," *Journal of Applied Physics*, vol. 113, no. 3, p. 034305, Jan. 2013. [Online]. Available: http://aip.scitation.org/doi/10.1063/1.4775406

[21] C. Daher, J. Torres, I. Iiguez-de-la-Torre, P. Nouvel, L. Varani, P. Sangar, G. Ducournau, C. Gaquire, J. Mateos, and T. Gonzlez, "Room Temperature Direct and Heterodyne Detection of 0.280.69-THz Waves Based on GaN 2-DEG Unipolar Nanochannels," *IEEE Transactions on Electron Devices*, vol. 63, no. 1, pp. 353–359, Jan. 2016.

[22] K. Takatani, T. Nozawa, T. Oka, H. Kawamura, and K. Sakuno, "AlGaN/GaN Schottky-ohmic combined anode field effect diode with fluoride-based plasma treatment," *Electronics Letters; Stevenage*, vol. 44, no. 4, pp. 1–2, Feb. 2008. [Online]. Available: https://search.proquest.com/docview/1625956443/abstract/6CDCC3888DE4DB4PQ/1

[23] Q. Zhou, W. Chen, C. Zhou, B. Zhang, and K. J. Chen, "High sensitivity AlGaN/GaN lateral field-effect rectifier for zero-bias microwave detection," *Electronics Letters*, vol. 49, no. 22, pp. 1391–1393, Oct. 2013.

[24] K. Wong, W. Chen, Q. Zhou, and K. J. Chen, "Zero-Bias Mixer Based on AlGaN/GaN Lateral Field-Effect Diodes for High-Temperature Wireless Sensor and RFID Applications," *IEEE Transactions on Electron Devices*, vol. 56, no. 12, pp. 2888–2894, Dec. 2009.

[25] W. Chen, K.-Y. Wong, W. Huang, and K. J. Chen, "High-performance AlGaNGaN lateral field-effect rectifiers compatible with high electron mobility transistors," *Applied Physics Letters*, vol. 92, no. 25, p. 253501, Jun. 2008. [Online]. Available: http://aip.scitation.org/doi/10.1063/1.2951615

[26] B. Lu, E. Matioli, and T. Palacios, "Tri-Gate Normally-Off GaN Power MISFET," *IEEE Electron Device Letters*, vol. 33, no. 3, pp. 360–362, Mar. 2012.

[27] R. G. Meyers, P. Fay, J. N. Schulman, S. Thomas, D. H. Chow, J. Zinck, Y. K. Boegeman, and P. Deelman, "Bias and temperature dependence of Sb-based heterostructure millimeter-wave detectors with improved sensitivity," *IEEE Electron Device Letters*, vol. 25, no. 1, pp. 4–6, Jan. 2004.

[28] S. Murad, "Dry etching damage in IIIV semiconductors," *Journal of Vacuum Science & Technology B: Microelectronics and Nanometer Structures*, vol. 14, no. 6, p. 3658, Nov. 1996. [Online]. Available: http://scitation.aip.org/content/avs/journal/jvstb/14/6/10.1116/1.588745

[29] J. Ma and E. Matioli, "Slanted Tri-Gates for High-Voltage GaN Power Devices," *IEEE Electron Device Letters*, vol. 38, no. 9, pp. 1305–1308, Sep. 2017.

[30] G. Santoruvo and E. Matioli, "In-Plane-Gate GaN Transistors for High-Power RF Applications," *IEEE Electron Device Letters*, vol. 38, no. 10, pp. 1413–1416, Oct. 2017.

[31] Y. Jo, D. Son, D. Lee, C. Won, J. H. Seo, I. M. Kang, and J. Lee, "First demonstration of GaN-based vertical nanowire FET with top-down approach," in *2015 73rd Annual Device Research Conference (DRC)*, Jun. 2015, pp. 35–36.

[32] Y. W. Jo, D. H. Son, C. H. Won, K. S. Im, J. H. Seo, I. M. Kang, and J. H. Lee, "AlGaN/GaN FinFET With Extremely Broad Transconductance by Side-Wall Wet Etch," *IEEE Electron Device Letters*, vol. 36, no. 10, pp. 1008–1010, Oct. 2015.

[33] A. Westlund, "Self-Switching Diodes for Zero-Bias Terahertz Detection," Ph.D. dissertation, Chalmers University of Technology, Mar. 2015.

[34] Agilent-Technologies, "Square Law and Linear Detection," Nov. 1999. [Online]. Available: http://g3ynh.info/circuits/diode_data/AN986.pdf

[35] X. Zhang, J. Grajal, J. L. Vazquez-Roy, U. Radhakrishna, X. Wang, W. Chern, L. Zhou, Y. Lin, P.-C. Shen, X. Ji, X. Ling, A. Zubair, Y. Zhang, H. Wang, M. Dubey, J. Kong, M. Dresselhaus, and T. Palacios, "Two-dimensional MoS2-enabled flexible rectenna for Wi-Fi-band wireless energy harvesting," *Nature*, Jan. 2019. [Online]. Available: http://www.nature.com/articles/s41586-019-0892-1

[36] A. Westlund, P. Sangar, G. Ducournau, I. Iiguez-de-la Torre, P.-. Nilsson, C. Gaquire, L. Desplanque, X. Wallart, J. Millithaler, T. Gonzlez, J. Mateos, and J. Grahn, "Optimization and small-signal modeling of zero-bias InAs self-switching diode detectors," *Solid-State Electronics*, vol. 104, pp. 79–85, Feb. 2015. [Online]. Available: http://linkinghub.elsevier.com/retrieve/pii/S0038110114002822